Journal of The
Electrochemical Society

Impact of Pressure Distribution and Magnitude on the Performance of Lithium Metal Anodes

To cite this article: John Shea *et al* 2024 *J. Electrochem. Soc.* **171** 020528

Journal of The Electrochemical Society, 2024 **171** 020528

Impact of Pressure Distribution and Magnitude on the Performance of Lithium Metal Anodes

John Shea,[1,2,3] Xiaozhou Huang,[1,2] Matthew Li,[1,z] Seoung-Bum Son,[1] Chi-Cheung Su,[1] Tongchao Liu,[1] Pei Dong,[2] Anna Chen,[4] Li Yang,[5] Chao Luo,[3,6] Khalil Amine,[1,z] and Umamaheswari Janakiraman[5,z]

[1]*Chemical Sciences and Engineering Division, Argonne National Laboratory, Lemont, Illinois 60439, United States of America*
[2]*Department of Mechanical Engineering, George Mason University, Fairfax, Virginia 22030, United States of America*
[3]*Department of Chemistry and Biochemistry, George Mason University, Fairfax, Virginia 22030, United States of America*
[4]*Laurel Heights Secondary School, Waterloo, ON, N2V 2V1, Canada*
[5]*Advanced Battery Cell Engineering, General Motors, Warren, Michigan 48093, United States of America*
[6]*Department of Chemical, Environmental, and Materials Engineering, University of Miami, Coral Gables, Florida 33146, United States of America*

Li metal anodes are a critical battery technology due to their ability to substantially increase the energy density of Li-based batteries. It is well known that pressure greatly impacts the performance of a Li-metal anode. However, precisely how the pressure value and distribution of pressure affect performance is unclear. Furthermore, the solid-electrolyte interphase composition that forms under varying pressure distributions remains a key parameter for practical lithium metal anodes. In this work, different pressure distributions were employed by using differently shaped and oriented mechanical springs in the coin cells, resulting in varying contact points. Pressure-sensitive films were used to spatially map the pressure and correlate it to the performance. It was found that higher average pressure does not necessarily have a positive effect on performance. When high pressure is paired with poor pressure uniformity, the performance is in fact worse likely due to the current focusing effect, rendering unsatisfied cycling stability. This work points to the importance of controlling the relationship between average pressure and pressure uniformity.
 [DOI: 10.1149/1945-7111/ad2648]

Manuscript submitted December 8, 2023; revised manuscript received January 25, 2024. Published February 15, 2024.
Supplementary material for this article is available online

Li metal anodes have become a very important technology for increasing the energy density of Li-based batteries. In comparison to the commercialized graphite anode, lithium metal exhibits a 10 times higher theoretical capacity of 3860 mAh g^{-1}. Unfortunately, many challenges occur when shifting from an intercalation storage mechanism (as in the case of graphite) to an electroplating or electrostripping mechanism. Problems such as dendritic lithium formation and continuous formation of solid-electrolyte-interphase (SEI) seriously impede the commercialization of such an anode. Dendritic lithium is derived from the Li-ion concentration gradient in the electrolyte that progressively shifts further away from the anode, bringing the position for lithium plating further and further away from the anode and closer to the cathode. Once the dendrites reach the cathode, the cell short circuits, resulting in a potential battery explosion. While this only appreciably occurs at higher current densities, the second challenge revolves around the continuous SEI growth, which deteriorates the cell by the constant consumption of electrolyte. In contrast to graphite, stable passivation layers are much more difficult to form over lithium metal due to the constant stripping and plating processes. As the degradation of the electrolyte is related to the surface area of the plated lithium metal, the morphology of the plated lithium directly dictates the degree of electrolyte degradation.

It is well known that the pressure of the cell greatly impacts the performance of the battery[1–3] drawing interest from numerous groups.[4,5] At higher pressures, the plating properties of lithium metals tend to form less dendritic morphology and favor smoother lithium metal plating. The smoother form of lithium metal formation is beneficial due to the decreased contact area between lithium metal surfaces and liquid electrolyte, resulting in less continuous SEI formation.[6,7] Recently, an increase in pressure uniformity and the use of $LiAsF_6$ as an electrolyte additive showed improvements in performance.[8] However, it is unclear as to the combined impact of pressure distribution and pressure magnitude on performance, Li metal plating morphology, and SEI composition.

In this work, we aim to answer these questions by using pressure-sensitive films to spatially map the pressure experienced inside the cell. Using a carbonate-based electrolyte Gen-II with 2 wt% vinylene carbonate (VC), the pressure was correlated with electrochemical performance (coulombic efficiency and symmetric cell cycling), revealing that performance is strongly dependent on pressure homogeneity. Surprisingly, we found that overall average (spatially) pressure correlated negatively with performance. A series of X-ray photoelectron spectroscopy and scanning electron microscopy at different radial distances from the center of the Li electrodes were employed to understand the impact of the pressure distribution on SEI composition and Li plating morphology. From our analysis, we determined that the outcome of a few standard electrochemical tests for Li metal anodes can be altered just by simply changing the type of spring. The higher-pressure regions produced lithium plating that was akin to the morphology associated in literature with higher current density plating, indicating the existence of a current focusing effect. This work reveals the impact of pressure distribution and magnitude on the cycling performance of lithium metal anode and aims to further our understanding of this anode technology.

Experimental

Electrochemical test.—Type 2032-coin cells were fabricated in an argon filled glove box for electrochemical performance testing and crimped using an automatic coin cell crimper purchased from Hohsen Corp. All cells used 16 mm diameter lithium metal chips of 100 μm, Entek Ceramic-Coated Separator, and 40 μl of electrolyte was used. The electrolyte composed of 1.2 M $LiPF_6$ in ethylene carbonate and ethyl methyl carbonate at a ratio of 3:7 with 2% vinylene carbonate for all cells. All electrochemical testing was done on a NEWARE cycler. For cycle life testing, the Li||Li cells were charged and discharged in a temperature-controlled chamber at a constant temperature of 25 °C. The Charge-Discharge testing was done at a rate of 0.18 mA cm^{-2} for an initial 4 cycles at a capacity

[z]E-mail: matthew.li@anl.gov; amine@anl.gov; uma.viswanathan@gm.com

stop of 1.8 mAh cm^{-2} and 0.36 mA cm^{-2} for the long-term cycling at a capacity limit of 1.8 mAh cm^{-2} and also a potential cutoff of −1.5 to 1.5 V. For coulombic efficiency measurements, 1.5 mAh cm^{-2} was first plated onto the Cu foil (15 mm diameter) followed by a stripping to 1.0 V using 0.4 mA cm^{-2}. A subsequent 1.5 mAh cm^{-2} was plated onto the Cu and used as the reservoirs, this is denoted as Qt. To follow 0.125 mAh cm^{-2} (denoted as Qc) was repeatedly stripped and plated at 0.4 mA cm^{-2} for 10 cycles. Finally, the Li on the Cu was stripped at a current of 0.4 mA cm^{-2} up to 1.0 V. The capacity measured at this last step is denoted as Qs. The coulombic efficiency was calculated by equation by Adams et al. as shown in Method 2 in his publication[9] and shown in Eq. 1:

$$CE = (nQ_C + Qs)/(nQc + Qt) \quad [1]$$

Where n, Qc, Qt, and Qs is 10 cycles, 0.125 mAh cm^{-2}, 1.5 mAh cm^{-2}, and measured final stripping capacity, respectively.

Full cell testing was performed using the same electrolyte and a $LiNi_{0.6}Mn_{0.2}Co_{0.2}O_2$ based cathode obtained from Argonne's Cell Analysis, Modelling, and Prototyping (CAMP) facility. These cathode had a nominal areal capacity of 1.58 mAh cm^{-2} at C/10.

X-ray photoelectron spectroscopy (XPS).—XPS was performed on a Physical Electronics PHI 5000 VersaProbe II system photoelectron spectrometer at an operating pressure of 1×10^{-7} Torr. XPS samples were symmetric cells. The XPS-sampled electrode was the one that experienced the first plating and last stripping. Samples were cycled ten times before being disassembled and gently washed in dimethyl carbonate and dried under vacuum before transferring into the XPS through the Ar-glovebox-XPS transfer chamber.

Pressure maps.—Pressure was measured and mapped using a combination of 3 levels of Fuji Prescale Pressure Indicating Films at the Medium, Low, and SuperLow pressure regimes. Coin cells were made with varying spring types with Li metal but with the Fuji films in the place of the separator in symmetric Li/Li cells. The cells were left to rest overnight after fabrication and opened and scanned with a printer and compared to Fuji's pressure scale for estimating pressure distribution after converting both to grayscale. Three different springs were used. Belleville springs (purchased from MTI Corporation) with small diameter up (denoted as Volcano) and small diameter down (denoted as Bowl) and a wave springs (denoted as Wave).

Fractional counts were calculated by the following equation.—Equation 2:

$$FC_x = \frac{I_x}{\sum I_x} \quad [2]$$

Where FC_x is the fractional counter at radial point x, I_x is the valid non-saturated/underexposed intensity measured at point x and $\sum I_x$ is the sum of all measured valid I_x. This was done separately for each of the three level of pressure tapes.

Scanning electron microscopy.—Scanning electron microscopy (SEM) was performed on a JEOL IT800HL. SEM samples were taken from symmetric cells. One single plating cycle was performed, and the investigated electrode was the Li foil that was plated on. Samples were washed in a similar way to XPS and then transferred into a SEM quickly to reduce exposure from air. Four equally spaced points starting from the center to the edge were taken as points A, B, C, and D with A being the centermost position and D at the edge most position.

Results and Discussion

To achieve different pressure distributions, three different spring configurations were used in CR2032 coin cells. These springs consisted of a wave spring (denotated as Wave spring and schematically shown in Fig. 1a and a conical spring that is placed either with the smaller opening facing towards the outwards of the cell (denoted as Bowl Spring and schematically shown in Fig. 1b) or with the smaller opening facing inwards towards the inside of the cell (denoted as Volcano spring and schematically shown in Fig. 1c). These configurations can produce different distributions of pressure and pressure values. To quantify the pressure distribution and values, we employed pressure sensing tapes from Fuji that become darker as the pressure increases. Figure 1d shows a series of 3-D pressure distribution plots (digital scans of the original mono-color films can be found in Fig. S1) across the three spring configurations and with three different levels of pressure tapes in a coin cell setup. The pressure is represented by the color and height of the plots and saturated at certain regions for the Low (sensing regime: 2.44–9.79 MPa) sensing region of and SuperLow (sensing regime: 0.48–2.41 MPa) while the Medium (sensing regime: 9.79–49.02 MPa) Fuji pre-scale pressure sensitivity tape did not saturate. It should be noted that the pressure measured here can only be taken as the highest pressure experienced by the films. The highest pressure experienced will likely occur during cell crimping, after the applied pressure has been relieved, the actual stack pressure of the cell will likely reduce. Therefore, the magnitude of the pressure can only be taken in comparison with other cells in this work and not used as an absolute value to compare with stack pressure in other cell configurations (pouch cells).

By comparing the results across all three levels shown in Fig. 1, we can deduce the distribution and average magnitude of pressure across all three configurations. Evidently, the bowl spring possessed the largest pressure in the SuperLow range, with the other springs also having significant pressure across the radius of the film. The wave spring had the highest pressure as viewed by the Low range films, with an even distribution across the area of the film. However, Medium range film reveals that the high-pressure region (out of the detection range for the Low range film) is concentrated at the edge of the film with peaks of about 22–30 MPa. Qualitatively, the Volcano spring has the largest area of high pressure, followed by the Bowl and then the Wave spring. As the Volcano has the largest area of both high and low pressure, its pressure uniformity can be qualitatively determined to be the lowest, while the Bowl and Wave can be considered rather similar to one another apart from the Low region film which indicates that the Wave spring offers the most uniform pressure distribution out of the three.

Two standard and widespread electrochemical tests were used to correlate with the quantified pressure distribution and magnitude results. Coulombic efficiency and symmetric cell cycling were performed on all three types of coin cell configurations with at least three repeats per sample. Coulombic efficiency was performed using the method described by Adams et al.[9] where Li was first plated onto Cu fold and then fully stripped, followed by reservoir deposition and constant current cycling for a smaller capacity for 10 cycles, and ending with a final full strip protocol. The coulombic efficiency was calculated using Eq. 1 as described in the method section. Sample voltage profiles can be found in Fig. S2. Using this method, we determined that the coulombic efficiency increases from Volcano to Bowl to Wave spring, with an average coulombic efficiency (±confidence interval of 95%) of 81.0 ± 0.584, 94.39 ± 0.317, and 96.48 ± 0.724, respectively (individual cell CE can be found in Table S1. Even with no other experimental conditions changed, the cells exhibited very different coulombic efficiencies. Aligning with the results from CE measurements, the symmetric Li/Li cycling (Figs. S3a and S3b) of cells containing the Volcano springs also performed the worst out of the three in terms of cycle life. Taken together, it is apparent that simple changes in cell configurations can have an enormous impact on performance.

In order to understand the relationship between the large variation in electrochemical performance and pressure, we aim to quantify two key metrics derived from the pressure films: pressure distribution and average pressure. To estimate the pressure

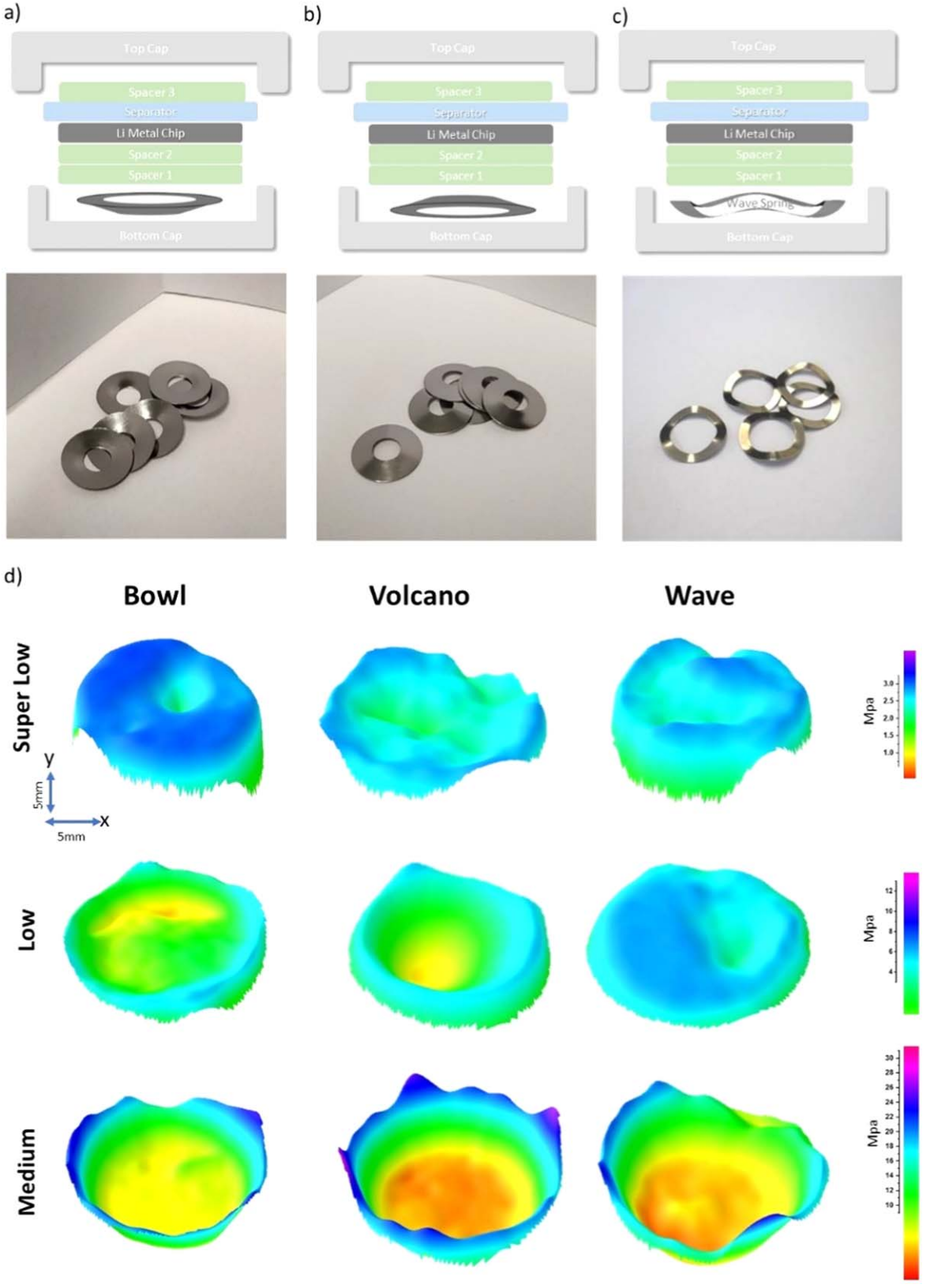

Figure 1. (a) Wave spring and Belleville spring from MTI in (b) Bowl position and (c) in Volcano position along with schematic of cell setup for each spring configuration. (d) Pressure distribution as measured using Fuji Prescale Pressure Films of three different pressure ranges: SuperLow, Low, and Medium films with their corresponding scale bar displayed to the right. Three different springs were tested Bowl, Volcano, and Wave (left, middle and right columns). Colors out of range of the pressure of the films are considered not accurate and not used in this manuscript.

distribution, we analyzed the standard deviation in the color histogram (when converted to grayscale) associated with the pressure films. A more uniform color map (lower standard deviation) will indicate a more uniform pressure distribution, and vice versa. The overall average pressure was calculated by the average darkness (color converted to grayscale) of the pressure tape. In order to obtain a quantitative correlation of the pressure distribution (standard deviation of the pressure color map) and average pressure magnitude (average value of the pressure color map) to the coulombic efficiency, we trimmed off the gray levels that were either over-saturated (upper pressure limit reached) or under-exposed (did not reach the lower pressure limit). Each of the three Fuji Prescale films: SuperLow (0.4–2.6 MPa), Low (3.6–11 MPa) and Medium (14–55 MPa) have their valid sensing pressure regimes. Because the number of valid counts (non-trimmed i.e. within the lower and upper pressure limits) varied with different pressure films, we calculated a "fractional count." By dividing the counts of each measured grayscale value with the number of total valid (non-trimmed) pixel counts of each pressure film, a direct comparison of fractional counts across different tapes can be performed (details in experimental section: Eq. 2). Figure 2a displays the compiled fractional counts of all three pressure films across all three springs. It should be noted that the discontinuities in the pressure regimes simply represent the inability of each film to accurately evaluate pressure levels outside of their sensing range. Looking at the pressure histogram, it is clear that similarities and differences are present for all the springs. Specifically, there appears to be a consistently high amount of pressure counts at around 2.5 MP, 10–12 MPa, and ~29–32 MPa. Different springs have different combinations of counts for these pressure regions, which is likely the cause of the observed differences in performances. For example, pressure values of ~5 MPa are mostly only present appreciably in the Bowl spring while the Wave spring has much higher counts in the 9–11 MPa region. Using this histogram, we can derive average pressure and standard deviation values (used to quantify uniformity) to correlate against coulombic efficiency for the different springs, taking into account all three levels of pressure (Fig. 2b).

Interestingly, when we averaged across all pressure film levels, the correlation between average pressure and uniformity with coulombic efficiency was very weak, seemingly suggesting a low dependency of the performance on the pressure distribution and magnitude. However, when standard deviation (Fig. 2c) and average pressure (Fig. 2d) values for each individual pressure sensing regime were separately plotted vs coulombic efficiency, we found very strong correlations ($R^2 = 0.98$ for standard deviation and $R^2 = 0.88$ for average pressure) at the Medium film (14–55 MPa) sensing regime. No significant correlation was found for the Low and SuperLow film sensing regimes. Interestingly, it appears that the

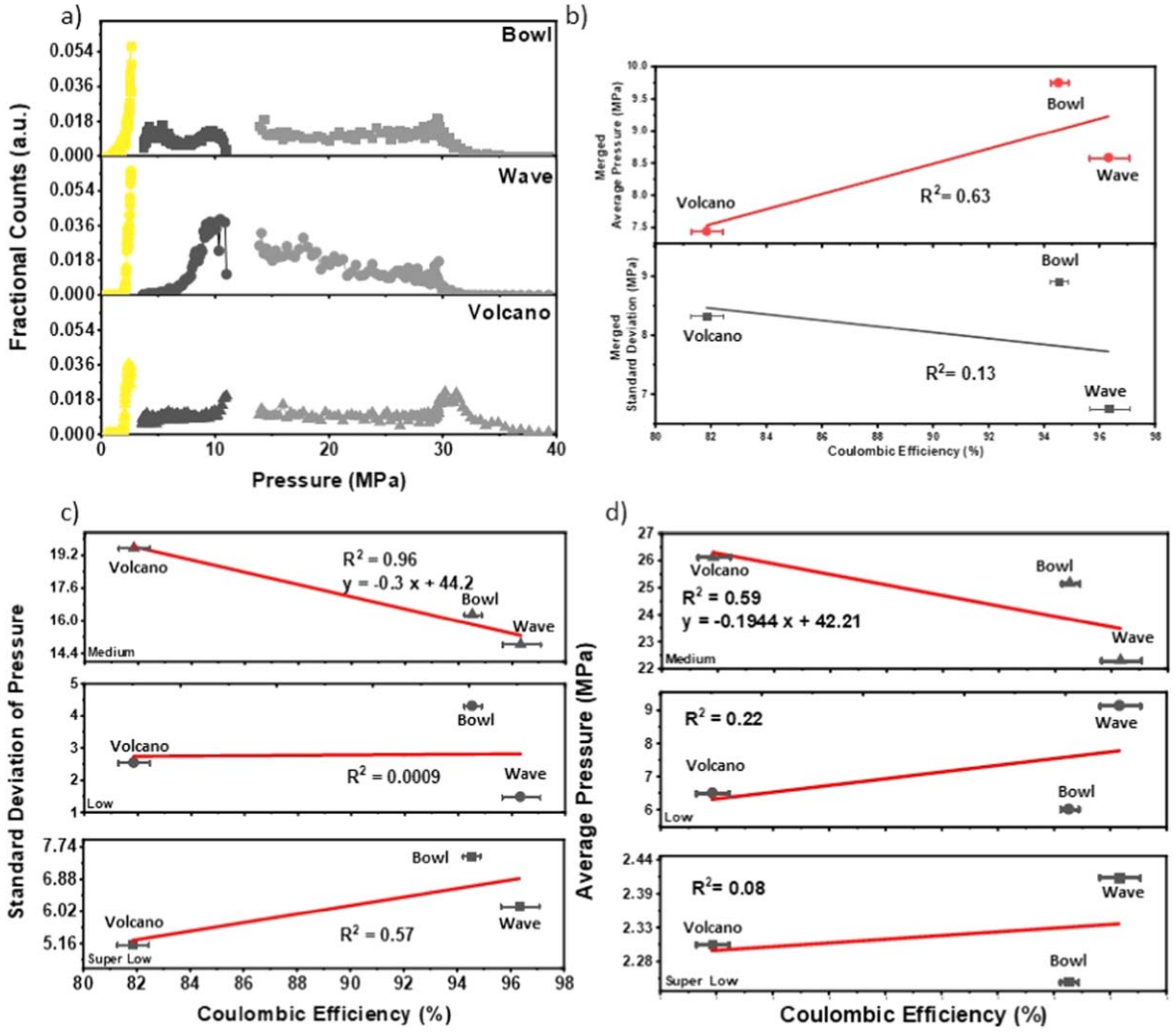

Figure 2. Merged pressure histogram of SuperLow (0.4–2.6 MPa), Low (3.6–11 MPa) and Medium (14–55 MPa) Fuji Prescale pressure sensitive films using Bowl, Wave and Volcano springs. (b) Relationship between the average pressure and standard deviation across all three tapes vs coulombic efficiency. Relationship between Coulombic efficiency and (c) Standard Deviation of Pressure and (d) Average pressure using the individual Medium, Low and SuperLow films with the lower and upper ranges trimmed to prevent artefact from under pressure and overpressure saturation. Error bar in the coulombic efficiency axis is based on a confidence interval of 95%.

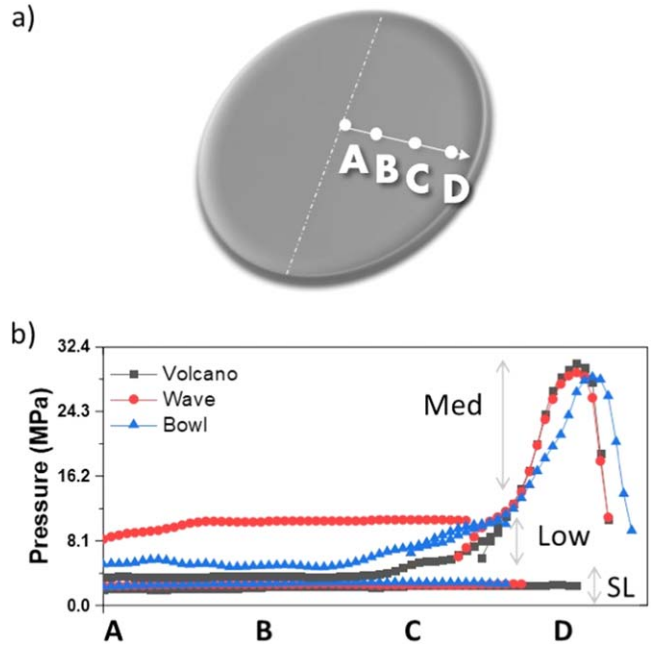

Figure 3. (a) Schematic illustrating the location of Position A, B, C, and D and (b) Pressure distribution as a function of position A, B, C, and D across all three sensing regimes and springs. The valid pressure sensing regions of each Prescale film is indicated as SuperLow (SL), Low, and Medium (Med).

contribution from the Low and SuperLow actually convoluted the pressure characteristics. From this analysis, we can conclude that the relatively higher-pressure regimes (14–55 MPa) are strongly related to coulombic efficiency, while the lower-pressure regimes are less important, or at least, their importance is overshadowed by the impact of the high-pressure areas. We believe this is due to a current focusing effect. The higher-pressure results in a better contact at these positions, leading to lower resistance and more current flow. The fact that the lower pressure areas are not correlated with performance suggests that there is some threshold pressure. It is likely that only above a certain threshold pressure will the stack pressure and its corresponding spatial distribution be impactful for performance.

Looking at the correlation with CE, the strong negative correlation between the standard deviation and CE is expected, as a more uniform pressure distribution will likely distribute the current more uniformly, preventing current hotspots. However, the average pressure measured also correlated negatively with CE. On the surface, this might appear contradictory to conventional understanding,[10–13] but can be likely explained by the trends observed in the uniformity. If the cell cannot distribute its pressure uniformly, an increase in average pressure will only exacerbate these non-uniformities. This will further amplify current hotspots and their associated negative impact on performance.

The source of this performance improvement was further investigated using a series of spatially resolved analyses on cycled lithium metal chips in symmetric cells. Analyzed cells were taken from the electrodes that finished at a plated protocol. We chose four positions on the lithium disc (schematically shown in Fig. 3a), from A-D with A and D at the center and edge of the Li disc, respectively, with equal spacing in between each position. Firstly, the pressure at each position was assumed to be roughly reflected in Fig. 3b. From the three different ranges of pressure films, we compiled a composite pressure profile as a function of radial distance (A-D). Pressure at the center was mostly interpreted using the Low range tape as the SuperLow tape was near saturation and considered unreliable. The Low range tape indicated that the pressure of Volcano spring was quite low (~4 MPa) in the A and B position. Bowl spring was slightly higher (>5 MPa). The wave spring exhibited the highest pressure in the A and B positions (>8.1 MPa). A similar trend was observed in position C. Position D indicates that the pressure was comparable between the three springs, but the Volcano spring appeared to be slightly higher than the others. At each of these positions, we performed morphological characterization to compare the shape of the deposited Li metal with pressure.

The plated Li metal morphology at different positions was studied under scanning electron microscopy (SEM). Figure 4 shows the morphology of Li metal plating at different positions (A) to (D) and with different springs. Morphologies typical to carbonate-based electrolyte systems such as moss-like, whisker-like, and tree-like (as per classification by Zuo et al.[14]) were found, indicating a wide range of governing processes. Such processes have been typically considered the combined effect of various parameter such as the nuclei states, mechanical properties of the Li deposits, mechanical property of the SEI and temperature. We find here that not only do these parameter effect the morphology but also the position and the experienced stack pressure. Clearly, the Li metal morphologies for the Bowl (Figs. 4a-d1), Volcano (Figs. 4e-h1), and Wave (Figs. 4i-l1) vary significantly across springs and, more importantly, are very positionally dependent. In contrast to the consensus that high surface area plating yields low CE, the correlation between the spatially resolved morphology and CE is much more complex than what has been considered. At Position A and B, the morphology of the Volcano spring's Li metal was not found to be as high-surface and porous as one would expect of deposits with a low CE. In fact, the plated Li metals at Position A are arguably the most uniform, with the Volcano spring (Figs. 4e-e1) versus the Bowl (Figs. 4a-a1) and the Wave springs (Figs. 4i-i1). Positions C and D are more in alignment with the performance; that is, the Volcano spring yielded thinner and more high surface area Li metal. This is further complicated by an unexpected relationship between pressure and deposition morphology. Position D (the edge) possesses the highest pressure spatially across the Li metal. When looking closely at the pressure experienced by Positions D (Fig. 3b), one can conclude that the Volcano spring has the largest pressure but produced the thinnest and least smooth Li metal morphology (Figs. 4h-h1) out of all the springs. This is rather surprising because higher pressure values have been consistently found to produce smoother and lower surface area Li plating.[8] These results can be explained by the existence of a non-uniform pressure distribution.

The notions that (1) better-performing (higher CE) Li anodes should yield lower surface area morphology and (2) higher pressure should yield more uniform Li morphology have been mostly based on total stack pressure and have, in fact, not looked into the impact on specific positions and pressure distribution. Although the Volcano spring has the highest average pressure, the distribution of pressure is very skewed due to the very high pressure experienced at Position D. Only Position D has a higher pressure than the other springs, while the other positions are in fact lower than the other springs. We believe the exclusively high pressure experienced by Position D in the Volcano spring created a region that had an amplified degree of contact and, as such, created a current focusing effect. Specifically, the Volcano spring experienced significantly higher than normal current density at Position D and Position A to C had their current densities progressively decrease as you moved towards the center. The higher current densities can cause the observed thinner and more moss like local Li metal plating[15–17] found in Figs. 4h and 4h1. Conversely, the smoother Li metal plating observed in Position A for the Volcano spring can be explained by a lower local current density near the center.

This effect was not found in the Bowl and Wave spring since its pressure values are more distributed than those of the Volcano spring. The result was smaller particles and higher surface area Li plating at Position A (center) for the Bowl and Wave springs over the Volcano. As one moves from Position B (off-center) towards Position C (near edge) the morphology of Volcano progressively begins to exhibit higher surface plating. This analysis can explain the counterintuitive negative correlation of CE with average measured

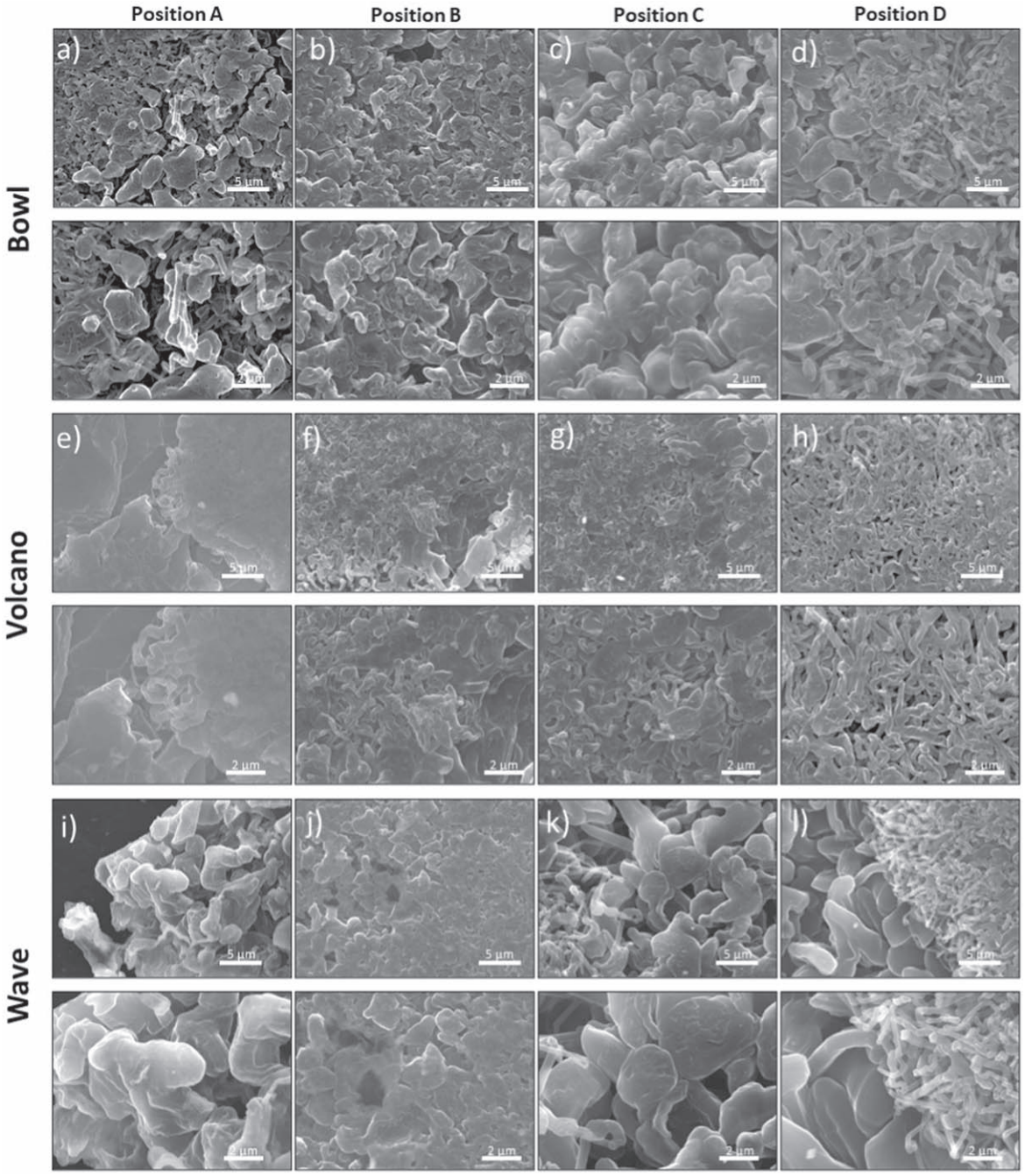

Figure 4. Scanning electron microscopy images of Li metal (1 cycle of stripping followed by plating using different springs and at different radial position from the center of the lithium metal foil with Position A followed by B, C and D towards the edge. Bowl spring: Figures (a)–(d) for position A, B, C, and D, respectively. Volcano spring: Figures (e)–(h), for position A, B, C, and D, respectively, and Wave spring: Figures (i)–(l) for position A, B, C, and D, respectively. Note each position has a low (top panels) and high (bottom panels) magnifications.

pressure and the positive correlation of CE with pressure uniformity shown in Figs. 2c and 2d (for the Medium pressure film). It appears that although the Volcano spring has a higher overall average pressure, most of its pressure is focused on the edge and does not reach the center of the cell, causing a current focusing effect that effectively increases the current density at the edge. This, in turn, decreases the CE. In contrast, while the Bowl and Wave springs yield an overall lower average pressure, the pressure is more uniformly dispersed, leading to a more distributed current, a locally lower current density and, as such, a higher CE.

Different current densities are known to produce not only different Li metal morphologies but different SEI compositions as well.[18] Accordingly, an immediate corollary of a spatially variable current density is likely a corresponding variability in the composition of the SEI across the surface of the Li metal. To confirm this, we performed X-ray photoelectron spectroscopy (XPS) at different radial positions after 10 cycles to ensure a more developed SEI composition and for the Wave and Volcano springs (highest and lowest CE, respectively). Shown in Figs. 5a–5d are the atomic percentages of each element along with their fitted constituting bonds for Position A to D and for different springs. In general, following the morphological trends in SEM, the changes in SEI composition are also more drastic for the Volcano spring. This can be seen in the sudden increase in fluorine content and LiF abundance when moving from Position B and C (Fig. 5a) whereas the Wave spring possesses similar fluorine content and LiF proportions

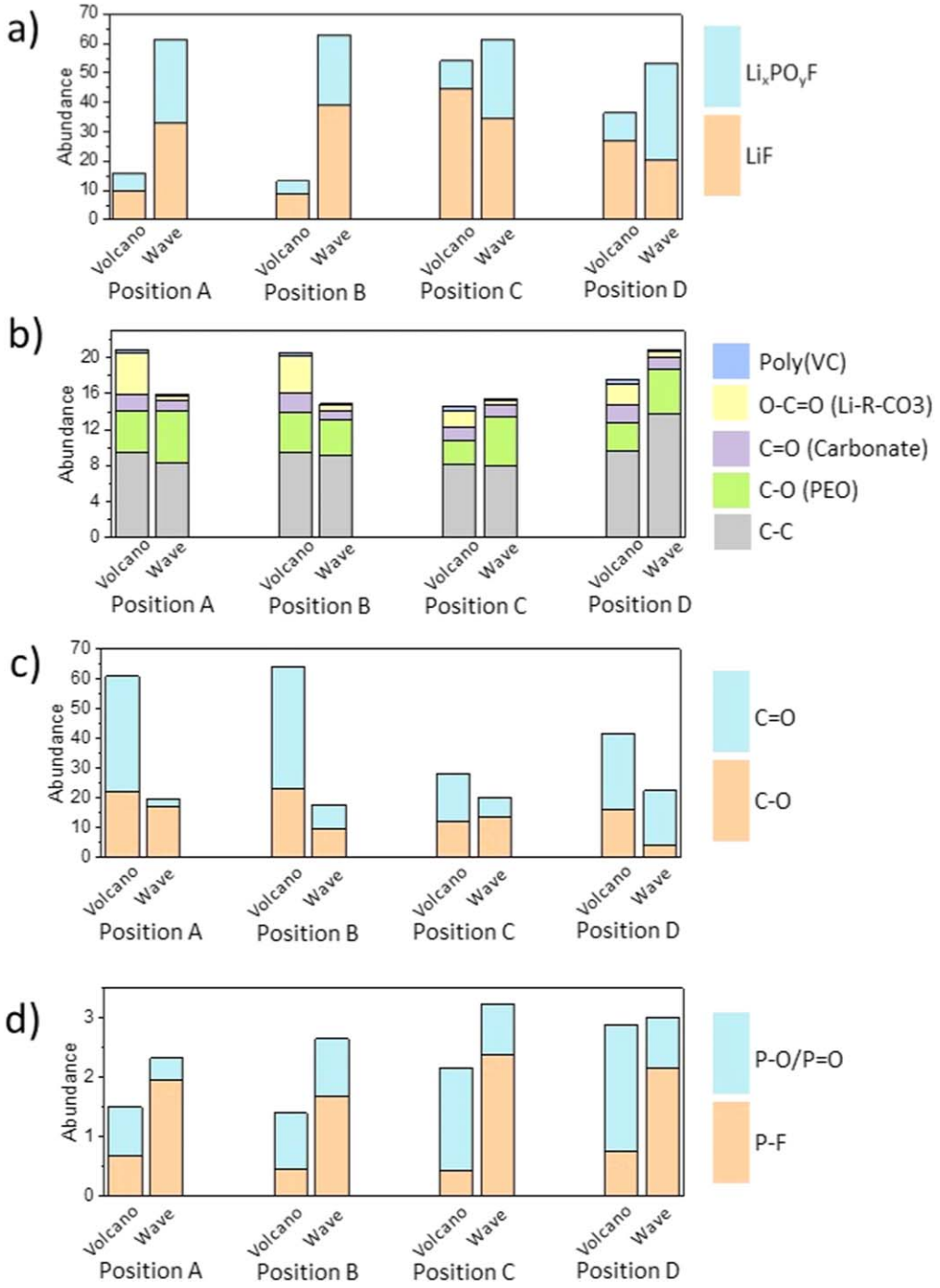

Figure 5. X-ray photoelectron spectroscopy. Atomic percentage of (a) fluorine, (b) carbon, (c) oxygen, and (d) phosphorus along with their fitted constituting bonds.

throughout. In fact, not only is the Wave spring more uniform in SEI composition across the four positions, but also possesses a higher amount of fluorine and phosphorus. Fluorine and phosphorus content are indications of $LiPF_6$ decomposition, generating LiF and $Li_xPO_yF_z$-like species. LiF, often considered a beneficial SEI component,[19] aligns well with the higher CE from the Wave spring. Interestingly, while this is true for Position A and B and arguably on average across the surface of the Li anode, the LiF content in Positions C and D, is actually slightly higher for the Volcano spring over the Wave (Fig. 5a). This is surprising, as the morphology at Position C and D has the thinnest Li metal fiber deposits for the Volcano spring. Although LiF content has been generally considered beneficial for performance, its role still remains unclear and is likely much more complex, and variation in its proportion does not always correlate with performance.[20–23]

One specific source of LiF content variation of relevance is the impact of current density. It has been found that the ratio of inorganic species to organic species on the surface varies with the applied current density, where a higher current density promotes inorganic species over the surface while lower current density has a more organic layer on the surface.[18] Interestingly, in the case of the Volcano spring, we see both situations where Positions A and B are richer in organic species, while Position C and D are richer in inorganic species (F-based species). This aligns with the proposed higher current density at the edge and lower current density at the center of the electrodes. The higher LiF content observed in Position

C and D is due to the higher local current density, which promotes LiF formation and therefore might not be a direct indication of the quality of the SEI.[18] On the other hand, a low local current density near the center produced a surface with more amorphous organic species in the SEI i.e. decreasing the observed LiF content on the surface.[18] In more detail, the abundance of organic species appears to be higher for the Volcano spring near the center of the Li foil, where the pressure is lower and, correspondingly, the current density. Higher levels of O-C=O (288.5 eV) and C=O (287.5 eV) were found, which correspond to lithium organic carbonates/lithium carbonate[23] and lithium ethylene dicarbonate[24] species, respectively. Surprisingly, polymerized VC was found to be in a similar and minimal proportion across both springs and all positions, indicating it is not responsible for the performance differences. It is possible that these carbonate species offer more favorable lithium deposition at low current densities.

The differing pressure likely changed the reaction rate between the Li metal and the electrolyte by changing both the surface area of Li metal and the local current density. Although both springs have a higher pressure at the edge (and a corresponding higher current density), the more uniform pressure distribution of the Wave spring appears to promote uniform SEI composition and likely contributed to the observed better electrochemical performances.

Conclusions

In conclusion, it is apparent that the impact of pressure value and uniformity are critical parameters for the performance of lithium metal batteries. A strong negative correlation was found between the average pressure vs coulombic efficiency, and a strong positive correlation was found between pressure uniformity (quantified by the standard deviation of color maps) vs coulombic efficiency. A current focusing effect was deduced from the differences in Li morphology, where we found that the Volcano spring (lowest CE) had a surprisingly smooth Li deposit near the center of the Li disc, where the pressure is the lowest, which suggests a lower current density. Conversely, at the edge where the pressure is the highest, the Li morphology is much more dendritic-like, indicating a much higher current than the other positions. X-ray photoelectron spectroscopy also reveals that the LiF and organic species in the Volcano spring exhibited much more variation radially across the Li disc. The Wave spring had a consistently high proportion of LiF while the Volcano spring had more organic species near the center (supposedly lower current density) and more inorganic species near the edge (supposedly higher current density). Such a trend between SEI composition and current density has been previously reported and supports our case of a current focusing effect.

Taken together, these results suggest that higher pressure might not always improve performance, as non-uniformities in the pressure distribution (and correspondingly, the local current density) can be amplified by a higher pressure. This was seen in the case of the Volcano spring, which simultaneously possessed the highest average pressure, lowest uniformity, and lowest coulombic efficiency.

We also wanted to point out that this spatial inhomogeneity in SEI composition was also previously reported by Oyakhire et al.[25] and was ultimately associated with the non-homogenous nature of the Li metal's SEI. However, we believe that the observed SEI surface inhomogeneity is a symptom of, or at least exacerbated by, different local current densities produced by the non-uniform pressure distribution often observed in coin cells and should be taken into consideration in future coin-cell based evaluation of Li metal anodes. Using rigid plates that do not deform under pressure would be an excellent method for increasing pressure uniformity. Clearly, the commonly used spacers in CR2032-type coin cells cannot serve this role, demanding perhaps thicker spacers as a solution.

Acknowledgments

The authors would like to acknowledge support from General Motors Inc. and the US Department of Energy (DOE), Office of Energy Efficiency and Renewable Energy, Vehicle Technologies Office. Argonne National Laboratory is operated by the DOE Office of Science by UChicago Argonne, LLC, under contract number DE-AC02–06CH11357. Work performed (Scanning electron microscopy) at the Center for Nanoscale Materials, a U.S. Department of Energy Office of Science User Facility, was supported by the U.S. DOE, Office of Basic Energy Sciences, under Contract No. DE-AC02–06CH11357.

ORCID

John Shea https://orcid.org/0000-0003-2146-2477
Matthew Li https://orcid.org/0000-0001-9093-3207
Seoung-Bum Son https://orcid.org/0000-0002-3723-6186
Chi-Cheung Su https://orcid.org/0000-0001-5675-3173
Chao Luo https://orcid.org/0000-0001-8497-8548

References

1. J.-M. Doux, H. Nguyen, D. H. S. Tan, A. Banerjee, X. Wang, E. A. Wu, C. Jo, H. Yang, and Y. S. Meng, "Stack pressure considerations for room-temperature all-solid-state lithium metal batteries." *Adv. Energy Mater.*, **10**, 1903253 (2020).
2. S. Chen, J. Zhang, L. Nie, X. Hu, Y. Huang, Y. Yu, and W. Liu, "All-solid-state batteries with a limited lithium metal anode at room temperature using a garnet-based electrolyte." *Adv. Mater.*, **33**, 2002325 (2021).
3. W. Cao, Q. Li, X. Yu, and H. Li, "Controlling Li deposition below the interface." *eScience*, **2**, 47 (2022).
4. W. Liu, Y. Luo, Y. Hu, Z. Chen, Q. Wang, Y. Chen, N. Iqbal, and D. Mitlin, "Interrelation between external pressure, sei structure, and electrodeposit morphology in an anode-free lithium metal battery." *Adv. Energy Mater.*, 2302261 (2023).
5. Y. Zhang, Y. Li, Z. Guo, J. Li, X. Ge, Q. Sun, Z. Yan, Z. Li, and Y. Huang, "Health monitoring by optical fiber sensing technology for rechargeable batteries." *eScience*, **4**, 100174 (2023).
6. L. Qin, K. Wang, H. Xu, M. Zhou, G. Yu, C. Liu, Z. Sun, and J. Chen, "The role of mechanical pressure on dendritic surface toward stable lithium metal anode." *Nano Energy*, **77**, 105098 (2020).
7. H. Liu, X. Sun, X.-B. Cheng, C. Guo, F. Yu, W. Bao, T. Wang, J. Li, and Q. Zhang, "Working principles of lithium metal anode in pouch cells." *Adv. Energy Mater.*, **12**, 2202518 (2022).
8. R. M. Kasse, N. R. Geise, E. Sebti, K. Lim, C. J. Takacs, C. Cao, H.-G. Steinrück, and M. F. Toney, "Combined effects of uniform applied pressure and electrolyte additives in lithium-metal batteries." *ACS Appl. Energy Mater.*, **5**, 8273 (2022).
9. B. D. Adams, J. Zheng, X. Ren, W. Xu, and J.-G. Zhang, "Accurate determination of coulombic efficiency for lithium metal anodes and lithium metal batteries." *Adv. Energy Mater.*, **8**, 1702097 (2018).
10. X. Yin, W. Tang, I. D. Jung, K. C. Phua, S. Adams, S. W. Lee, and G. W. Zheng, "Insights into morphological evolution and cycling behaviour of lithium metal anode under mechanical pressure." *Nano Energy*, **50**, 659 (2018).
11. L. Qian et al., "Critical operation strategies toward high-performance lithium metal batteries." *Renewables*, **1**, 114 (2023).
12. T. Hirai, I. Yoshimatsu, and J. I. Yamaki, "Influence of electrolyte on lithium cycling efficiency with pressurized electrode stack." *J. Electrochem. Soc.*, **141**, 611 (1994).
13. C. Fang et al., "Pressure-tailored lithium deposition and dissolution in lithium metal batteries." *Nat. Energy*, **6**, 987 (2021).
14. P. Zou, Y. Sui, H. Zhan, C. Wang, H. L. Xin, H.-M. Cheng, F. Kang, and C. Yang, "Polymorph evolution mechanisms and regulation strategies of lithium metal anode under multiphysical fields." *Chem. Rev.*, **121**, 5986 (2021).
15. L. Frenck, G. K. Sethi, J. A. Maslyn, and N. P. Balsara, "Factors that control the formation of dendrites and other morphologies on lithium metal anodes." *Frontiers in Energy Research*, **7** (2019).
16. R. L. Sacci, J. M. Black, N. Balke, N. J. Dudney, K. L. More, and R. R. Unocic, "Nanoscale imaging of fundamental li battery chemistry: solid-electrolyte interphase formation and preferential growth of lithium metal nanoclusters." *Nano Lett.*, **15**, 2011 (2015).
17. K. Dong et al., "Unravelling the mechanism of lithium nucleation and growth and the interaction with the solid electrolyte interface." *ACS Energy Lett.*, **6**, 1719 (2021).
18. Y. Xu, H. Wu, H. Jia, J.-G. Zhang, W. Xu, and C. Wang, "Current density regulated atomic to nanoscale process on li deposition and solid electrolyte interphase revealed by cryogenic transmission electron microscopy." *ACS Nano*, **14**, 8766 (2020).
19. J. Ko and Y. S. Yoon, "Recent progress in lif materials for safe lithium metal anode of rechargeable batteries: is lif the key to commercializing li metal batteries?" *Ceram. Int.*, **45**, 30 (2019).

20. W. Huang, H. Wang, D. T. Boyle, Y. Li, and Y. Cui, "Resolving nanoscopic and mesoscopic heterogeneity of fluorinated species in battery solid-electrolyte interphases by cryogenic electron microscopy." *ACS Energy Lett.*, **5**, 1128 (2020).
21. H. Kuwata, H. Sonoki, M. Matsui, Y. Matsuda, and N. Imanishi, "Surface layer and morphology of lithium metal electrodes." *Electrochemistry*, **84**, 854 (2016).
22. Z. L. Brown, S. Jurng, and B. L. Lucht, "Investigation of the lithium solid electrolyte interphase in vinylene carbonate electrolytes using Cu||Lifepo4 cells." *J. Electrochem. Soc.*, **164**, A2186 (2017).
23. H. Ota, Y. Sakata, A. Inoue, and S. Yamaguchi, "Analysis of vinylene carbonate derived sei layers on graphite anode." *J. Electrochem. Soc.*, **151**, A1659 (2004).
24. G. V. Zhuang, K. Xu, H. Yang, T. R. Jow, and P. N. Ross, "Lithium ethylene dicarbonate identified as the primary product of chemical and electrochemical reduction of Ec in 1.2 M Lipf6/Ec:Emc electrolyte." *J. Phys. Chem. B*, **109**, 17567 (2005).
25. S. T. Oyakhire, H. Gong, Y. Cui, Z. Bao, and S. F. Bent, "An X-ray photoelectron spectroscopy primer for solid electrolyte interphase characterization in lithium metal anodes." *ACS Energy Lett.*, **7**, 2540 (2022).